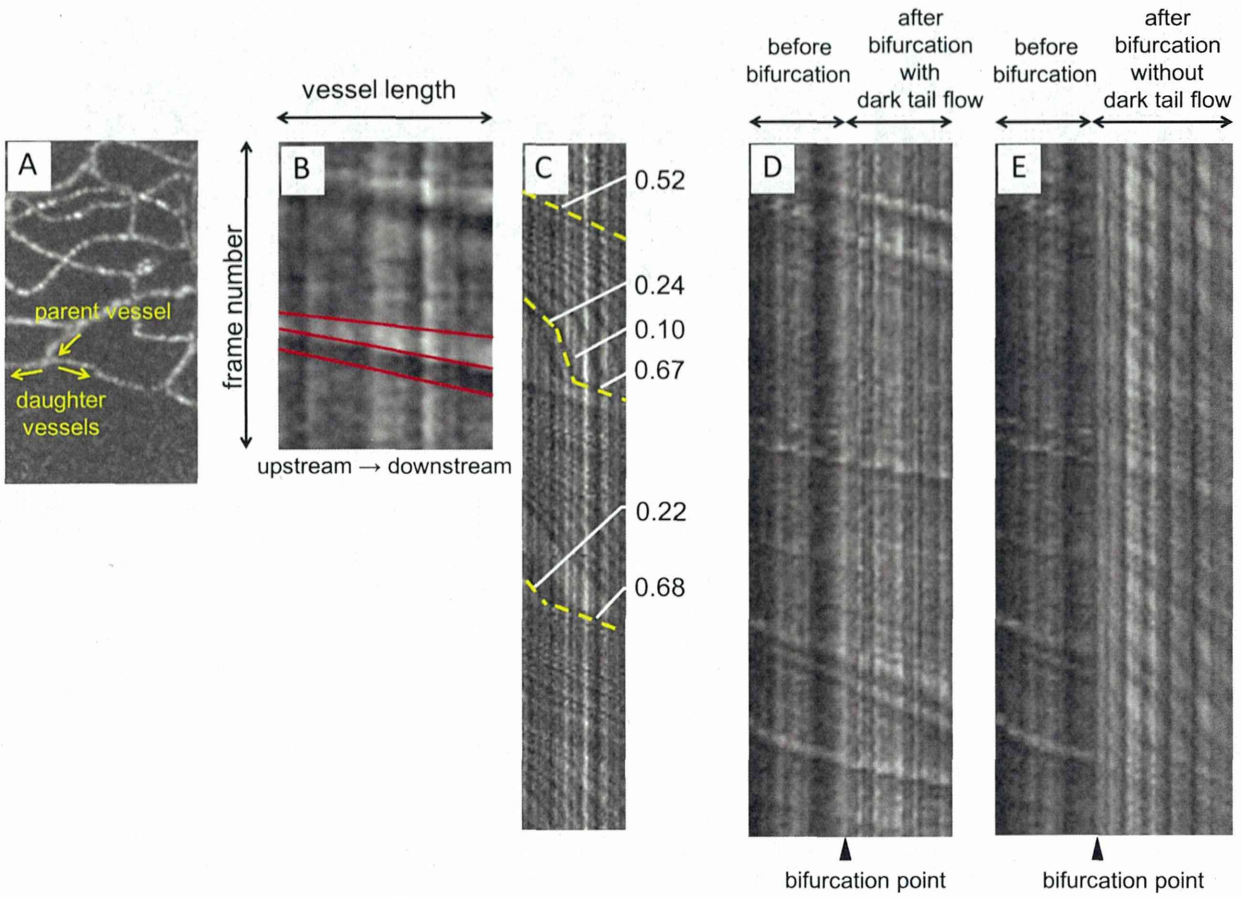

Figure 3. Interpretation and characteristics of spatiotemporal (ST) images. (A) Vessels before bifurcation were defined as parent vessels. Vessels after bifurcation were defined as daughter vessels. (B) Interpretation of ST images. Vessels with a dark tail, a white band, and a dark band were observed. The narrow white band corresponded to trajectories of bright moving objects, and the wide black band corresponded to trajectories of the dark tail. Dark tail velocity was calculated as the slope of the red line placed halfway between white and dark bands. As velocity decreased, the slope steepened. (C) An ST image of a vessel without a dark tail. Curved velocity changes were observed. Unlike vessels with a dark tail, velocities were not straight lines and seemed to change periodically (velocity varied between 0.10 and 0.68 mm/s over 2 s in this ST image). Numbers on the right side are yellow slope velocities showing changes every moment. (D) Combined ST images of dark tail vessels before and after bifurcation. (E) Combined ST images of a dark tail parent vessel and a non-dark tail daughter vessel. Sudden velocity decreases were observed at bifurcations.
doi:10.1371/journal.pone.0089679.g003

performed by using StatView (ver. 5.0, SAS Inc., Cary, NC). A p value <0.05 was considered statistically significant.

Results

Distribution of Pathways Preferential to Dark Tails

Mean subject age was 33.4±7.1 years (range, 23–41 years) and mean axial length was 24.8±1.2 mm (range, 23.6–26.5). In all 5 subjects, vessels could be divided into 2 groups based on the presence or absence of dark tail flow. The average length of dark tail vessels for 3 days was 3077±191 μm, and the average length of non-dark tail vessels was 4926±180 μm in Subject A. These numbers varied between subjects and measured 5192±272 and 3755±263 μm in Subject B; 3301±99 and 7327±106 μm in Subject C; 3150±11 and 5110±53 μm in Subject D; and 3566±17 and 3118±2 μm in Subject E, for dark tail and non-dark tail vessels, respectively (Figure 4A). The average lengths of dark tail vessels and non-dark tail vessels at the FAZ boundary, respectively, were 1360±12 and 844±5 μm in Subject A; 1362±20 and 1014±20 μm in Subject B; 727±12 and 2579±29 μm in Subject C; 766±16 and 1500±47 μm in Subject D; and 1444±17 and 576±2 μm in Subject E (Figure 4A). No significant pathway differences were found between dark tail flow and non-dark tail flow vessel groups in the measured region 150 μm away from the FAZ ($p = 0.29$) or at the FAZ boundary ($p = 0.75$).

Variation in Dark Tail Flow Distribution

On the 3 different days that AO-SLO images were collected, only minimal variation in dark tail flow distribution was observed between measurements in 4 subjects (Figure 4B). In Subject A, distribution changes were found in 2 vessels among 3 measurements (from 1 branch to another). These distribution changes were also found in 3 vessels in Subject B and in 4 vessels each in Subjects C and D. In subject E, no changes were observed. Changes in the direction of dark tail flow were not observed in any subject.

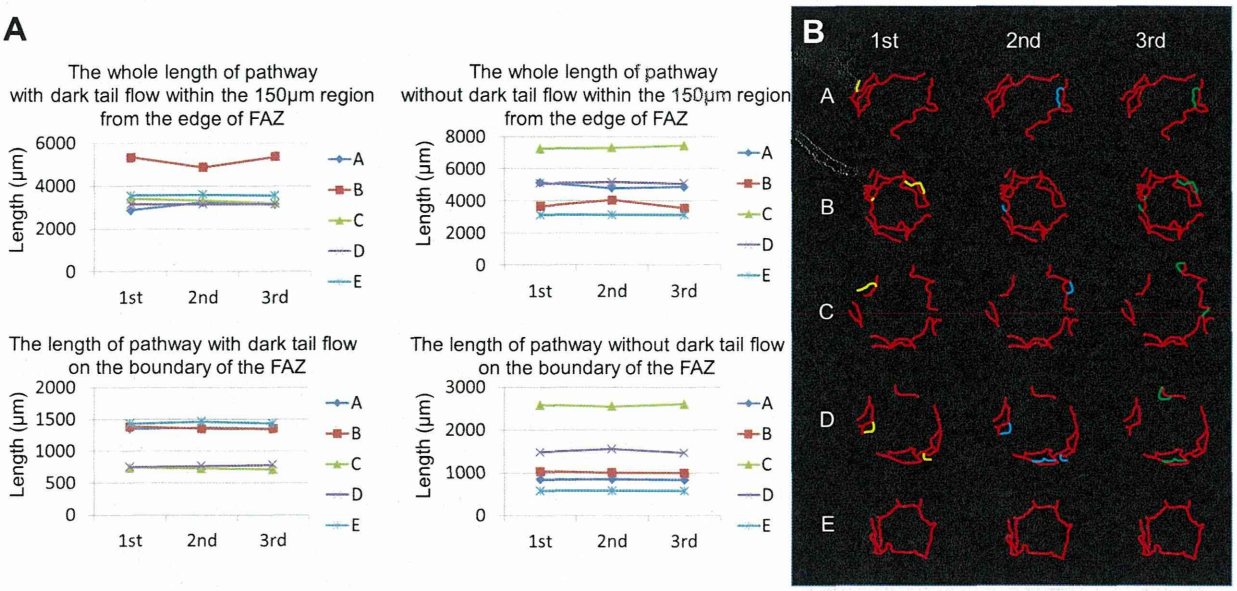

Figure 4. Daily variance of dark tail flow distribution. (A) Changes in the lengths of pathways with or without dark tail on three different days. Note that the lengths show little daily variance. Alphabet A, B, C, D, and E represent each subject. (B) Blood flow distributions of dark tails in the parafovea were nearly identical on each of 3 different days, with only minimal changes in 4 of 5 subjects. Red lines represent the same distribution of dark tails on the 3 different days. The yellow, blue, and green lines represent differences in distribution between days.
doi:10.1371/journal.pone.0089679.g004

Differences between Pathways with and without Dark Tail Flow on Spatiotemporal Images

On pathways with a dark tail flow, a narrow white band and a wide black band, which represented a bright moving object's and a dark tail's trajectory, respectively, were observed on ST images. The trajectories of both bands were straight lines. On pathways without a dark tail flow, dense bands were seen and had curved trajectories (Figure 3).

Blood Flow Velocity in Pathways with and without Dark Tail Flow at a Bifurcation

A total of 48 bifurcation points, where dark tail flow bisected into a dark tail and a dark tail-free flow, were analyzed. Additionally, a total of 96 dark tails and 48 plasma gaps were analyzed in 5 normal subjects to examine velocity differences in moving objects between the parent vessel and the 2 daughter vessels. The average velocity of dark tails was 1.30±0.27 mm/s (range, 0.59–2.11) in parent vessels and 1.12±0.25 mm/s (range, 0.61–1.98) in daughter vessels with dark tails ($p = 0.003$) (Table 1). When velocity measurements were averaged in both types of vessels, dark tail velocity was 1.21±0.26 mm/s. The average velocity of plasma gaps in daughter vessels without a dark tail was 0.64±0.11 mm/s (range, 0.26–1.13), which was significantly lower than dark tail velocity in both the parent ($p<0.001$) and daughter ($p<0.001$) vessels.

Bifurcation Vessel Diameter and Angle of Pathways with and without Dark Tail Flow

The average vessel diameters of parent vessels, daughter vessels with dark tail flow, and daughter vessels without dark tail flow were 8.4±1.6 μm, 8.7±1.6 μm, and 8.6±1.9 μm, respectively (Table 1). The average vessel diameter was not significantly different in parent vessels and in daughter vessels with ($p = 1.0$) or without ($p = 1.0$) dark tail flow. There was also no difference between daughter vessels with and without dark tail flow ($p = 1.0$). The average angle between parent and daughter vessels with dark tail flow was 43.6°, and the angle between parent and daughter vessels without dark tail flow was 86.9°(Table 1). The angle between parent and daughter vessels with a dark tail flow was significantly smaller than the angle between parent and daughter vessel without a dark tail flow ($p<0.0001$).

Discussion

In this study, erythrocyte aggregates were observed as dark tails on AO-SLO images. The distribution of dark tails in the parafoveal capillary network and their behavior at vessel bifurcations were explored in normal subjects. The AO-SLO imaging revealed two different pathways in the parafoveal capillary network; pathways with dark tails and pathways without dark tails. This suggests that erythrocyte aggregates have preferential pathways through the retinal microcirculation. Moreover, daughter vessels with dark tail flow formed smaller angles with parent vessels at bifurcation points and had higher blood velocities than daughter vessels without dark tail flow. Therefore, bifurcation angle and blood flow velocity may influence which path erythrocyte aggregates prefer.

Previous studies have focused on blood flow characterization in the retinal microcirculation, in which preferential leukocyte pathways were documented. Nishiwaki et al. [12] identified retinal leukocyte "preferential channels" in the rat, in which leukocytes predominantly flowed. These channels were characterized by a high flow velocity and a straight, short capillary route. These preference prevented leukocytes from entering small capillaries, where they would have likely become stuck. Tam et al. [18] found leukocyte-preferred paths (LPPs) and plasma gap capillaries (PGCs) in the human retinal circulation using AO-SLO. They theorized that LPPs might prevent leukocytes from entering non-

Table 1. Differences in average velocity, vessel diameter, and angle of bifurcation between the vessel before bifurcation, after bifurcation with dark tail flow, and after bifurcation without dark tail flow.

Subject	Average Velocity(mm/sec)				Average Diameter(μm)				Average Angle(degree)			
	Before bifurcation	After bifurcation with dark tail flow	After bifurcation without dark tail flow	P value	Before bifurcation	After bifurcation with dark tail flow	After bifurcation without dark tail flow	P value	After bifurcation with dark tail flow	After bifurcation without dark tail flow	P value
A	1.34±0.39	0.91±0.10	0.69±0.11		7.7±0.98	8.9±2.2	8.3±1.2		45.8±21.7	87.8±24.9	
B	0.92±0.21	1.12±0.35	0.47±0.17		8.2±1.7	7.8±1.2	7.9±1.1		37.9±25.6	100.2±15.5	
C	1.67±0.19	1.52±0.43	0.75±0.15		8.6±1.1	10±1.3	9.1±2.4		34.0±12.4	81.1±38.8	
D	1.26±0.24	1.16±0.17	0.71±0.17		8.9±3.0	7.8±1.3	8.1±2.1		51.7±43.2	84.5±24.6	
E	1.32±0.37	0.91±0.26	0.58±0.19		8.8±0.96	8.8±1.3	9.6±2.7		48.8±31.6	81.0±27.5	
Average	1.30±0.27	1.12±0.25	0.64±0.11	P<0.0001	8.4±1.6	8.7±1.6	8.6±1.9	P = 0.88	43.6±26.5	86.9±25.3	P<0.001

doi:10.1371/journal.pone.0089679.t001

LPP capillaries and that PGCs may serve as relief valves when a leukocyte enters a nearby LPP.

Our results are in agreement with the Tam et al. study. [18] The dark tail-free pathway was very similar to their PGCs. The difference was that they focused on bright particles, identified as leukocytes, while we focused on dark regions, identified as erythrocyte aggregates. They measured leukocyte speeds in LPP segments as 1.80 mm/s, which were significantly higher than plasma gaps in PGC segments (1.30 mm/s), but not in LPP segments (1.73 mm/s). Although we did not analyze plasma gap velocity in dark tail pathways, which are smaller and likely heavily influenced by both erythrocyte aggregates and leukocytes, we did examine plasma gaps in dark tail-free pathways. The observed differences between reports may have been caused by inherent study differences. Firstly, their data was obtained from 1 healthy subject. Secondly, we measured plasma gap velocity only in vessels without dark tail flow. As Figure 3C shows, extremely slow velocities were included in analyses of vessels without dark tail flow.

Following bifurcation, blood flow velocity in daughter vessels with dark tail flow (range, 0.61–1.98 mm/s) was significantly higher than in daughter vessels without dark tail flow (range, 0.26–1.13 mm/s). In addition, velocities within vessels without dark tails were more variable. Figure 3C shows ST images of vessels without dark tail flow. The ST images consisted of both straight and curved lines, and the curved lines may represent periodical velocity change. The range of velocities measured from Figure 3C varied between 0.10 and 0.68 mm/s and included extremely slow blood flow in vessels without dark tail flow. One of the possible causes of these slow flow velocities was the influence of pulsation. As indicated in Figure 3, trajectories on the ST images showed a regular cycle of changing in slope, suggesting that pulsation changed the velocity of blood components periodically. All of these observations suggest that blood flow velocity evaluation in the parafoveal capillary network can account for velocity differences in vessels with and without dark tail flow, which should be analyzed separately.

The results showed great variability in the length of dark tail vessels among the subjects. One possible reason for this variability is the wide interindividual variability in the size of the FAZ. Because the areas of analysis were determined on the basis of the FAZ boundary in order to extract the area with the capillary monolayer, total extension of the vessels might be substantially influenced by FAZ size. On the other hand, dark tail flow distribution varied slightly between images recorded on separate days. As shown in Figure 4, even when different pathways existed, some commonality was present. These slight pathway changes were likely caused by flow frequency, not by absolute blood flow. Therefore, the current study showed that erythrocyte aggregates have preferential pathways and that this preference has minimal change.

The hemodynamics of erythrocyte aggregates could be a potential biomarker of microcirculatory disturbance in vascular diseases. Hemorheological disturbances (e.g., decreased erythrocyte deformability [33] and increased erythrocyte aggregation [31], [32]) are known to occur in diabetics and are thought to be associated with erythrocyte hyperaggregation, which would promote pathologic blood flow distribution in nutritive capillaries. [34] Erythrocyte aggregation also increases in patients with systemic lupus erythematosus (SLE), which could decrease blood flow and contribute to thromboembolitic processes in SLE patients. [35] Future investigations on erythrocyte aggregate flow frequency and distribution in parafoveal capillaries of diseased eyes are planned.

Because erythrocytes and leukocytes move in a single file and erythrocytes cannot overtake leukocytes in the capillary lumen, we assumed that the dark tail head velocity was approximately that of leukocytes. In support of this assumption, average dark tail velocity in retinal capillaries was close to that of leukocytes, as measured by Martin et al. [19], [28] with AO-SLO, who reported an average leukocyte velocity of 1.37 mm/s [28] and 1.30 mm/s. [19] However, values obtained in the current study were considerably lower than those that we obtained in a previous study (1.49 mm/s). [22] This difference may have been caused by differences in vessels examined and by variation between data selection. In the current study, we chose series of vessels, which consisted of 1 parent and 2 daughter vessels, but in our previous study, we chose vessels at random, regardless of bifurcation influence. Another explanation could be the influence of cardiac cycle on blood flow on velocity, as reported by Martin et al. [19] and Zhong et al. [27] Measurement of pulsatility would reveal cyclic changes in blood flow velocity, which would make calculations of mean velocity more accurate. We did not assess the pulsatility cardiac cycle in our previous report, but this was done in the current study.

Our study had several limitations due to the relatively low number of bifurcations analyzed and image resolution. Several different patterns of blood flow occurred at bifurcations, as observed on AO-SLO images, and only vessels consisting of a parent vessel and a daughter vessel with and without dark tails were chosen for analysis. This decreased the number of bifurcations meeting inclusion criteria to 48.

In conclusion, AO-SLO noninvasively revealed the existence of pathways with and without dark tail flow in normal subjects. Pathways with dark tail flow in daughter vessels had a faster blood flow and a smaller bifurcation angle than daughter vessels without dark tail flow. Therefore, AO-SLO is an informative tool for examining retinal microcirculatory hemodynamics.

Acknowledgments

This study was presented in part at the Association for Research in Vision and Ophthalmology (ARVO) meeting in Seattle, Washington, in May 2013.

Author Contributions

Conceived and designed the experiments: SA AU SO KM NY. Performed the experiments: SA AU. Analyzed the data: SA AU. Contributed reagents/materials/analysis tools: SA AU SO KM NY. Wrote the paper: SA AU.

References

1. Cheung CY, Ikram MK, Sabanayagam C, Wong TY (2012) Retinal microvasculature as a model to study the manifestations of hypertension. Hypertension 60: 1094–1103.
2. Ritt M, Schmieder RE (2009) Wall-to-lumen ratio of retinal arterioles as a tool to assess vascular changes. Hypertension 54: 384–387.
3. Keith NM, Wagener HP, Barker NW (1974) Some different types of essential hypertension: their course and prognosis. Am J Med Sci 268: 336–345.
4. Scheie HG (1953) Evaluation of ophthalmoscopic changes of hypertension and arteriolar sclerosis. AMA Arch Ophthalmol 49: 117–138.
5. Burgansky-Eliash Z, Barak A, Barash H, Nelson DA, Pupko O, et al. (2012) Increased retinal blood flow velocity in patients with early diabetes mellitus. Retina 32: 112–119.
6. Riva CE, Grunwald JE, Sinclair SH, Petrig BL (1985) Blood velocity and volumetric flow rate in human retinal vessels. Invest Ophthalmol Vis Sci 26: 1124–1132.
7. Ott C, Raff U, Harazny JM, Michelson G, Schmieder RE (2013) Central pulse pressure is an independent determinant of vascular remodeling in the retinal circulation. Hypertension 61: 1340–1345.
8. Sugiyama T, Araie M, Riva CE, Schmetterer L, Orgul S (2010) Use of laser speckle flowgraphy in ocular blood flow research. Acta Ophthalmol 88: 723–729.
9. Burgansky-Eliash Z, Nelson DA, Bar-Tal OP, Lowenstein A, Grinvald A, et al. (2010) Reduced retinal blood flow velocity in diabetic retinopathy. Retina 30: 765–773.
10. Srinivasan VJ, Radhakrishnan H, Lo EH, Mandeville ET, Jiang JY, et al. (2012) OCT methods for capillary velocimetry. Biomed Opt Express 3: 612–629.
11. Nishiwaki H, Ogura Y, Kimura H, Kiryu J, Honda Y (1995) Quantitative evaluation of leukocyte dynamics in retinal microcirculation. Invest Ophthalmol Vis Sci 36: 123–130.
12. Nishiwaki H, Ogura Y, Kimura H, Kiryu J, Miyamoto K, et al. (1996) Visualization and quantitative analysis of leukocyte dynamics in retinal microcirculation of rats. Invest Ophthalmol Vis Sci 37: 1341–1347.
13. Miyamoto K, Hiroshiba N, Tsujikawa A, Ogura Y (1998) In vivo demonstration of increased leukocyte entrapment in retinal microcirculation of diabetic rats. Invest Ophthalmol Vis Sci 39: 2190–2194.
14. Kimura H, Kiryu J, Nishiwaki H, Ogura Y (1995) A new fluorescent imaging procedure in vivo for evaluation of the retinal microcirculation in rats. Curr Eye Res 14: 223–228.
15. Cooper RF, Dubis AM, Pavaskar A, Rha J, Dubra A, et al. (2011) Spatial and temporal variation of rod photoreceptor reflectance in the human retina. Biomed Opt Express 2: 2577–2589.
16. Merino D, Duncan JL, Tiruveedhula P, Roorda A (2011) Observation of cone and rod photoreceptors in normal subjects and patients using a new generation adaptive optics scanning laser ophthalmoscope. Biomed Opt Express 2: 2189–2201.
17. Takayama K, Ooto S, Hangai M, Ueda-Arakawa N, Yoshida S, et al. (2013) High-resolution imaging of retinal nerve fiber bundles in glaucoma using adaptive optics scanning laser ophthalmoscopy. Am J Ophthalmol 155: 870–881.
18. Tam J, Tiruveedhula P, Roorda A (2011) Characterization of single-file flow through human retinal parafoveal capillaries using an adaptive optics scanning laser ophthalmoscope. Biomed Opt Express 2: 781–793.
19. Martin JA, Roorda A (2009) Pulsatility of parafoveal capillary leukocytes. Exp Eye Res 88: 356–360.
20. Bedggood P, Metha A (2012) Direct visualization and characterization of erythrocyte flow in human retinal capillaries. Biomed Opt Express 3: 3264–3277.
21. Uji A, Hangai M, Ooto S, Takayama K, Arakawa N, et al. (2012) The source of moving particles in parafoveal capillaries detected by adaptive optics scanning laser ophthalmoscopy. Invest Ophthalmol Vis Sci 53: 171–178.
22. Arichika S, Uji A, Hangai M, Ooto S, Yoshimura N (2013) Noninvasive and direct monitoring of erythrocyte aggregates in human retinal microvasculature using adaptive optics scanning laser ophthalmoscopy. Invest Ophthalmol Vis Sci 54: 4394–4402.
23. Chui TY, Vannasdale DA, Burns SA (2012) The use of forward scatter to improve retinal vascular imaging with an adaptive optics scanning laser ophthalmoscope. Biomed Opt Express 3: 2537–2549.
24. Tam J, Dhamdhere KP, Tiruveedhula P, Manzanera S, Barez S, et al. (2011) Disruption of the retinal parafoveal capillary network in type 2 diabetes before the onset of diabetic retinopathy. Invest Ophthalmol Vis Sci 52: 9257–9266.
25. Tam J, Martin JA, Roorda A (2010) Noninvasive visualization and analysis of parafoveal capillaries in humans. Invest Ophthalmol Vis Sci 51: 1691–1698.
26. Tam J, Roorda A (2011) Speed quantification and tracking of moving objects in adaptive optics scanning laser ophthalmoscopy. J Biomed Opt 16: 036002.
27. Zhong Z, Song H, Chui TY, Petrig BL, Burns SA (2011) Noninvasive measurements and analysis of blood velocity profiles in human retinal vessels. Invest Ophthalmol Vis Sci 52: 4151–4157.
28. Martin JA, Roorda A (2005) Direct and noninvasive assessment of parafoveal capillary leukocyte velocity. Ophthalmology 112: 2219–2224.
29. Demiroglu H (1997) The importance of erythrocyte aggregation in blood rheology: considerations on the pathophysiology of thrombotic disorders. Blood 89: 4236.
30. Puniyani RR, Ajmani R, Kale PA (1991) Risk factors evaluation in some cardiovascular diseases. J Biomed Eng 13: 441–443.
31. Babu N, Singh M (2005) Analysis of aggregation parameters of erythrocytes in diabetes mellitus. Clin Hemorheol Microcirc 32: 269–277.
32. Cho YI, Mooney MP, Cho DJ (2008) Hemorheological disorders in diabetes mellitus. J Diabetes Sci Technol 2: 1130–1138.
33. Le Devehat C, Khodabandehlou T, Vimeux M (2001) Impaired hemorheological properties in diabetic patients with lower limb arterial ischaemia. Clin Hemorheol Microcirc 25: 43–48.
34. Singh M, Shin S (2009) Changes in erythrocyte aggregation and deformability in diabetes mellitus: a brief review. Indian J Exp Biol 47: 7–15.
35. Spengler MI, Svetaz MJ, Leroux MB, Bertoluzzo SM, Carrara P, et al. (2011) Erythrocyte aggregation in patients with systemic lupus erythematosus. Clin Hemorheol Microcirc 47: 279–285.

Clinical Ophthalmology

Dovepress
open access to scientific and medical research

Open Access Full Text Article

CASE REPORT

Adaptive optics assisted visualization of thickened retinal arterial wall in a patient with controlled malignant hypertension

Shigeta Arichika
Akihito Uji
Nagahisa Yoshimura

Department of Ophthalmology and Visual Sciences, Graduate School of Medicine, Kyoto University, Kyoto, Japan

Purpose: We aimed to visualize the retinal arterial wall thickness, assisted by noninvasive adaptive optics scanning laser ophthalmoscopy (AO-SLO).

Methods: The arterial wall thickness was measured and compared between one normal subject and one patient suffering from malignant hypertensive retinopathy.

Results: Increased arterial wall thickness was revealed with a newly developed AO-SLO system, in a retinal artery of 1-papilla diameter temporal inferior to the optic disc. The average wall thickness, with hypertension, was 18.7 μm, and the wall-to-lumen ratio was 0.44, both bigger than normal.

Conclusion: AO-SLO enabled us to evaluate the retinal wall thickness in the hypertensive patient. The arterial walls were thickened compared with normal. AO-SLO may facilitate future noninvasive study of arterial walls in human medicine.

Keywords: wall thickness, AO-SLO, hypertensive retinopathy

Introduction

The Keith–Wagener[1] and Scheie[2] classification schemes are widely used for staging of hypertensive and arteriosclerotic changes, by categorizing vascular appearance on ophthalmoscopic examination or color fundus photography. Recently, direct visualization of the arterial walls in the retina using adaptive optics scanning laser ophthalmoscopy (AO-SLO) has been reported and is expected to provide valuable information on hypertensive and sclerotic arterial changes. Herein, we illustrate a case of malignant hypertension in which AO-SLO images clearly demonstrated a thickened retinal arterial wall.

Case report

A 33-year-old woman complaining of decreased vision in the right eye was referred to our institution. Her visual acuity was 20/50 in the right eye and 20/20 in the left eye. Fundus examination revealed retinal hemorrhage, "cotton-wool" spots, and papill-edema in both eyes, with macular edema in the right eye (Figure 1). Spectral-domain optical coherence tomography (SD-OCT) (Spectralis®; Heidelberg Engineering, Heidelberg, Germany) showed serous retinal detachment and hyperreflective foci, which represented precursors of hard exudate in the retina. Her blood pressure was 234/134 mmHg, and blood tests showed elevated serum creatinine level (14 mg/dL). Moreover, abdominal magnetic resonance imaging (MRI) revealed bilateral renal atrophy. She was diagnosed with malignant nephrosclerosis, malignant hypertension, and hypertensive retinopathy. Hemodialysis and antihypertensive treatment

Correspondence: Akihito Uji
Department of Ophthalmology and Visual Sciences, Kyoto University Graduate School of Medicine, 54 Kawahara-cho Shogoin, Sakyo-ku, Kyoto 606-8507, Japan
Tel +81 75 751 3248
Fax +81 75 752 0933
Email akihito1@kuhp.kyoto-u.ac.jp

submit your manuscript | www.dovepress.com
Dovepress
http://dx.doi.org/10.2147/OPTH.S71966

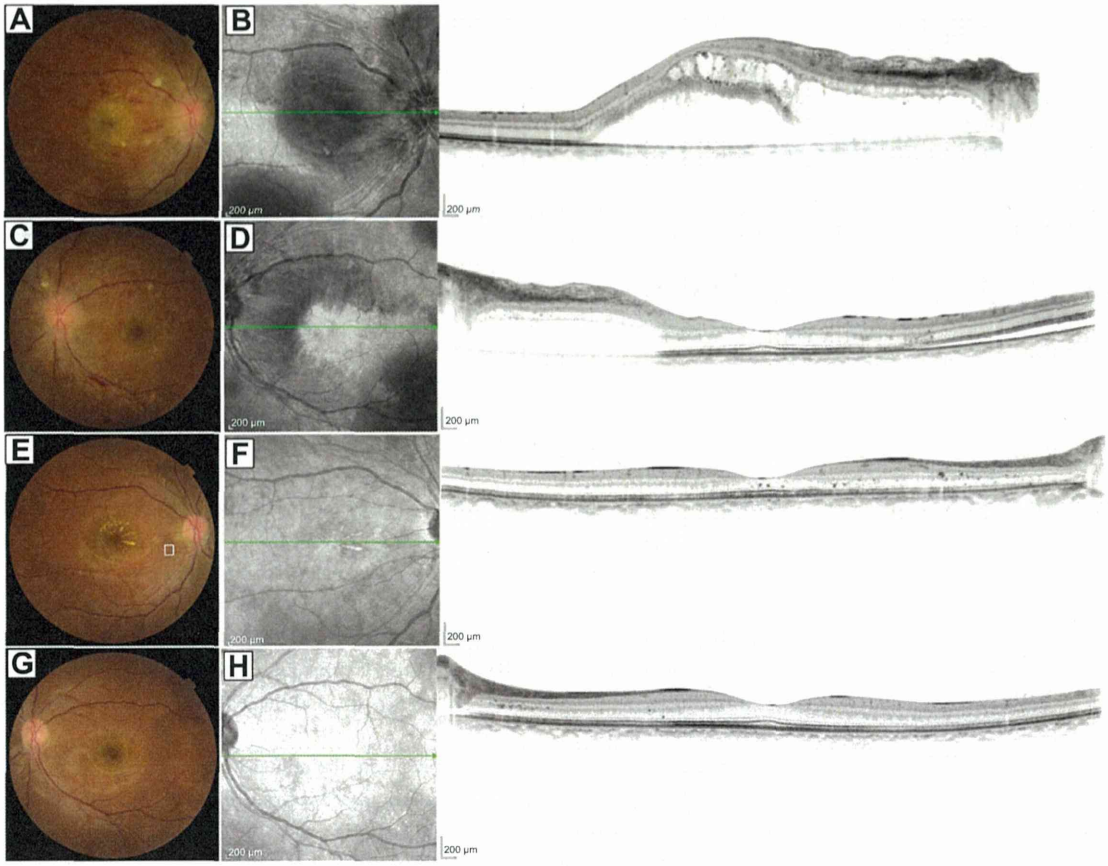

Figure 1 Fundus photographs and spectral-domain optical coherence tomography (SD-OCT) before and after treatment.
Notes: Images of both eyes of a 33-year-old woman with hypertensive retinopathy (**A**–**D**) before treatment and (**E**–**H**) 3 months after hypertensive treatment started. (**A**) Color photograph of the right eye shows retinal hemorrhage, "cotton-wool" spots, papilledema, and macular edema. (**B**) Horizontal line scan on SD-OCT of the right eye shows serous retinal detachment and hyperreflective foci, representing precursors of hard exudate in the retina. (**C**) Color photograph of the left eye shows retinal hemorrhage, cotton-wool spots, and papilledema, all of which are milder than those in the right eye. (**D**) Horizontal line scan on SD-OCT of the left eye shows serous retinal detachment and hyperreflective foci. (**E** and **G**) Fundus findings reveal favorable response to hypertensive treatment. (**F** and **H**) Horizontal line scans on SD-OCT of both eyes show complete disappearance of serous retinal detachment. The scale bar represents 200 µm. Green arrows represent the sectioned line of the SD-OCT.

were started immediately. Three months later, her blood pressure had decreased to 115/69, and abnormal findings, except for minimal deposition of hard exudate in the fundus, had resolved. Visual acuity in the right eye had improved to 20/16. Increased arterial wall thickness was revealed with an AO-SLO system (Canon Inc., Tokyo, Japan) in a retinal artery of 1-papilla diameter temporal inferior to the optic disc in the right eye (Figure 2). The average wall thickness was 18.7 µm, and the wall-to-lumen ratio was 0.44.

Adaptive optics scanning laser ophthalmoscopy

We developed a novel AO-SLO system with a high wavefront correction efficiency, using a dual liquid-crystal phase modulator (LCOS-SLM, model X10468-02; Hamamatsu Photonics, Hamamatsu City, Japan). The AO-SLO videos were acquired at 32 frames/second in an area covering the parafovea. The scan area was 2.8°×2.8° at the retina, with a sampling of 400×400 pixels. All AO-SLO imaging was performed with the optical focus adjusting on the vessel wall to be described clearly.

Discussion

AO-SLO is a useful modality for noninvasive demonstration of, not only photoreceptor cells, but also, blood flow, blood corpuscles, and the retinal nerve fiber layer. Recently, visualization of arterial wall thickness in the retina has been reported.[3] In the current report, AO-SLO yielded clear images of a vascular wall in a patient with controlled malignant hypertension and revealed thickening of the vessel wall compared with a normal volunteer of the same age as the patient. The wall-to-lumen ratio reported here concurred with previous

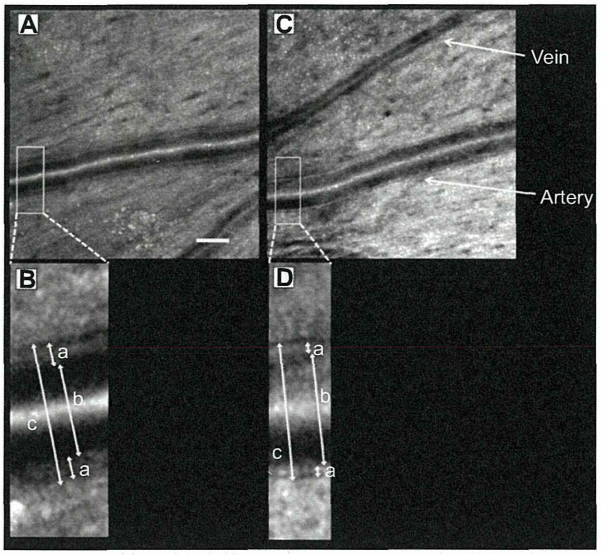

Figure 2 Adaptive optics scanning laser ophthalmoscopy (AO-SLO) images of thickened retinal arterial wall.

Notes: (**A**) AO-SLO image, corresponding to the area outlined in white in Figure 1E, of a retinal artery in controlled hypertensive retinopathy and (**B**) magnified image of the area outlined in white in (**A**). (**C**) AO-SLO image of a retinal artery temporal-superior to the optic disc in a normal subject and (**D**) magnified image of the area outlined in white in (**C**). (**A**) Scale bar = 100 μm. (**B**) The arterial wall (a) is thicker than that of the normal subject in (**D**). The average wall thickness (a), inner diameter (b), outer diameter (c), and wall-to-lumen ratio of the retinal artery were 18.7 μm, 86.2 μm, 123.7 μm, and 0.44, respectively. (**D**) The average wall thickness (a), inner diameter (b), outer diameter (c), and wall-to-lumen ratio of the retinal artery were 10.7 μm, 92.4 μm, 113.7 μm, and 0.23, respectively.

results obtained using Doppler flowmetry by Ritt et al[4] and Rizzoni et al[5] who reported wall-to-lumen ratios of 0.28 and 0.26, respectively, for normotensive subjects, and of 0.36 and 0.37, respectively, for hypertensive patients. The changes in arterial structure in hypertension are considered to result from mechanoadaptive processes to maintain optimum levels of wall tension or stress. Although blood pressure was well controlled in this patient, the arterial wall thickening suggested that blood vessel wall changes were irreversible to a certain extent. AO-SLO may facilitate future noninvasive study of arterial walls, in human medicine. In the near future, we intend to conduct further studies using an appropriate number of patients.

Acknowledgment

This work was supported in part by the Innovative Techno-Hub for Integrated Medical Bio-imaging Project of the Special Coordination Funds for Promoting Science and Technology, from the Ministry of Education, Culture, Sports, Science and Technology, Japan.

Disclosure

Nagahisa Yoshimura received lecture fees and research funding from Canon. The authors report no other conflicts of interest in this work.

References

1. Keith NM, Wagener HP, Barker NW. Some different types of essential hypertension: their course and prognosis. *Am J Med Sci*. 1974;268(6):336–345.
2. Scheie HG. Evaluation of ophthalmoscopic changes of hypertension and arteriolar sclerosis. *AMA Arch Ophthalmol*. 1953;49(2):117–138.
3. Chui TY, Vannasdale DA, Burns SA. The use of forward scatter to improve retinal vascular imaging with an adaptive optics scanning laser ophthalmoscope. *Biomed Opt Express*. 2012;3(10):2537–2549.
4. Ritt M, Harazny JM, Ott C, et al. Analysis of retinal arteriolar structure in never-treated patients with essential hypertension. *J Hypertens*. 2008;26(7):1427–1434.
5. Rizzoni D, Porteri E, Duse S, et al. Relationship between media-to-lumen ratio of subcutaneous small arteries and wall-to-lumen ratio of retinal arterioles evaluated noninvasively by scanning laser doppler flowmetry. *J Hypertens*. 2012;30(6):1169–1175.

Retinal Hemorheologic Characterization of Early-Stage Diabetic Retinopathy Using Adaptive Optics Scanning Laser Ophthalmoscopy

Shigeta Arichika, Akihito Uji, Tomoaki Murakami, Noriyuki Unoki, Shin Yoshitake, Yoko Dodo, Sotaro Ooto, Kazuaki Miyamoto, and Nagahisa Yoshimura

The Department of Ophthalmology and Visual Sciences, Kyoto University Graduate School of Medicine, Kyoto, Japan

Correspondence: Akihito Uji, Department of Ophthalmology and Visual Sciences, Kyoto University Graduate School of Medicine, 54 Shogoin Kawahara-cho, Sakyo-ku, Kyoto 606-8507, Japan; akihito1@kuhp.kyoto-u.ac.jp.

Submitted: June 26, 2014
Accepted: September 5, 2014

Citation: Arichika S, Uji A, Murakami T, et al. Retinal hemorheologic characterization of early-stage diabetic retinopathy using adaptive optics scanning laser ophthalmoscopy. *Invest Ophthalmol Vis Sci.* 2014;55:8513–8522. DOI:10.1167/iovs.14-15121

Purpose. Adaptive optics scanning laser ophthalmoscopy (AO-SLO) is a noninvasive technique that allows for the direct monitoring of erythrocyte aggregates in retinal capillaries. We analyzed the retinal hemorheologic characteristics in normal subjects, diabetic patients without diabetic retinopathy (NDR), and diabetic patients with nonproliferative diabetic retinopathy (NPDR), using spatiotemporal (ST) blood flow images to visualize blood corpuscle trajectory.

Methods. AO-SLO images of the parafoveal capillary network were acquired for three groups: 20 healthy volunteers, 17 diabetic patients with NDR (8 type 1 and 9 type 2 patients), and 10 diabetic patients with NPDR (4 type 1 and 6 type 2). The erythrocyte aggregate velocity assigned to a relative cardiac cycle and the elongation rate of the erythrocyte aggregate were calculated.

Results. Careful observation revealed that flow velocity fluctuations were found with higher frequency in diabetic patients than in normal subjects. The total average velocities were 1.26 ± 0.22 mm/s in the normal group, 1.31 ± 0.21 mm/s in the NDR group, and 1.63 ± 0.35 mm/s in the NPDR group. The average velocities of the NPDR group were higher than those in the normal ($P = 0.001$) and NDR ($P = 0.009$) groups. The average elongation rates of the 3 groups were 0.67 ± 0.20, 0.39 ± 0.19, and 0.33 ± 0.11, respectively. Elongation rate differed significantly between the normal and NDR ($P = 0.003$) groups as well as the normal and NPDR ($P = 0.001$) groups.

Conclusions. AO-SLO can be used to detect retinal hemorheologic changes in the early stages of diabetic retinopathy.

Keywords: diabetic retinopathy, AO-SLO, hemorheology

Diabetic retinopathy (DR) is a leading cause of blindness.[1,2] Because the early detection of DR is important in the prevention of DR progression[3,4] as well as cardiovascular events[5–7] and stroke,[7] effective tools with which to screen for DR are needed. Fundus examinations by ophthalmoscopy and color fundus photography have long been considered the gold standards for diagnosing and staging DR. Although imaging technology in the field of ophthalmology, including optical coherence tomography (OCT), has advanced rapidly in recent decades, no other useful method for the diagnosis of DR has been established for the detection of signs that appear earlier than the microaneurysm (MA), the earliest clinical sign[8] detectable by routine fundus examination. The ability to detect microlesions secondary to DR before the manifestation of clinically apparent retinopathy would improve the patient's visual prognosis and quality of life.

The pathogenesis of DR is characterized by histopathologic changes, such as a loss of pericytes,[9] endothelial cell death,[9,10] thickening of the basement membrane,[9] and leukocyte adherence to the retinal vascular endothelium,[10] as well as hemorheologic changes, such as reduced leukocyte deformability,[11] reduced erythrocyte deformability,[12,13] increased erythrocyte aggregation,[12,14,15] and increased platelet aggregation.[16] In order to analyze abnormal hemodynamics with the potential to elucidate pathologic changes other than clinically detectable morphological changes in DR, retinal blood flow measurements were obtained using various techniques and at various stages of type 1 and type 2 DR. The technologies presented here will facilitate research on DR as well as other types of retina pathophysiology.[17,18] Their development is therefore believed to be capable of catalyzing dramatic breakthroughs in the development of tools for the early diagnosis of retinal disorders.

Erythrocytes play an important role in the hemorheology of vascular disease.[12,13,19] Erythrocyte aggregation is considered to be an important hemorheologic parameter in DR because the increase in erythrocyte aggregation[12–14] prevents erythrocytes from passing through the capillaries.[13] Further investigations of retinal hemodynamics at the level of the capillary are needed. To date, the gold standard for evaluating human retinal capillaries has been fluorescein angiography, which carries a risk of allergic reaction.

Adaptive optics scanning laser ophthalmoscopy (AO-SLO) is a promising technology that can be used to image the retinal microvasculature noninvasively, objectively, and directly (Fig. 1).[20–28] Adaptive optics allows the researcher to correct for

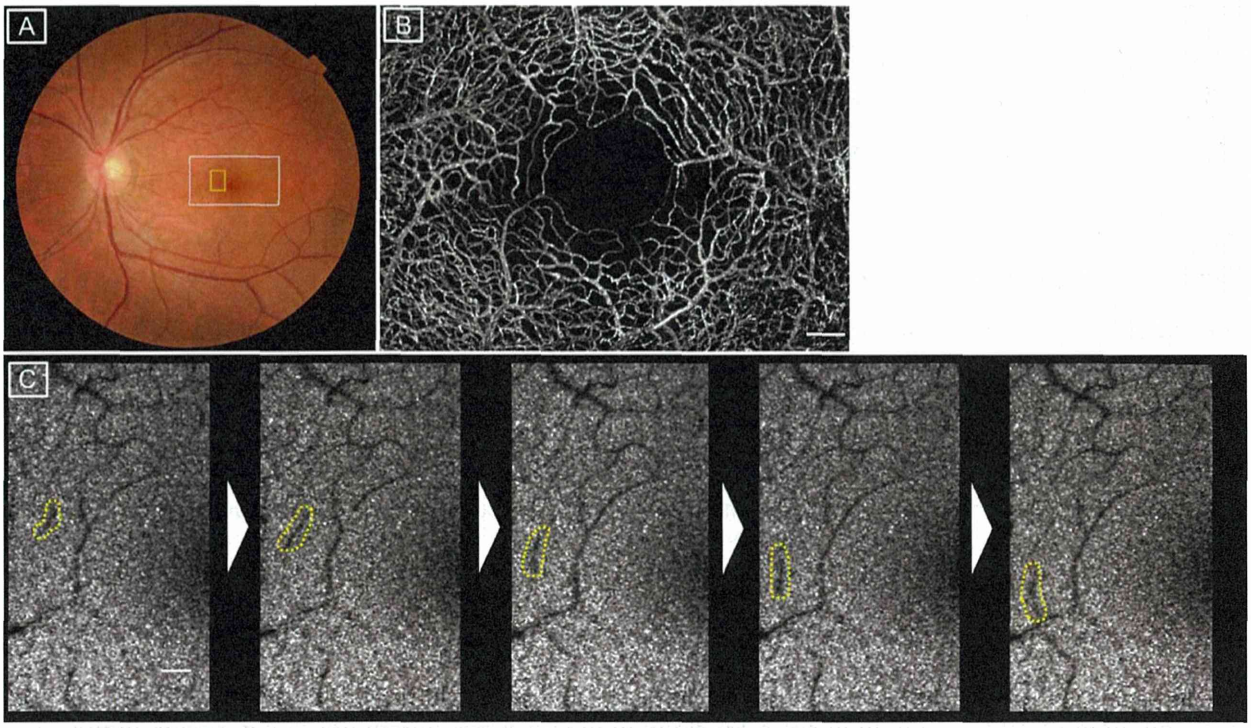

FIGURE 1. Microcirculation network information detected by AO-SLO. (**A**) Fundus photograph of the left eye in a normal subject. (**B**) Montage of the foveal microvasculature (perfusion map) obtained noninvasively by using the motion contrast-enhancement technique from AO-SLO images without any dying agents. The montage corresponds to the *white* outlined area in the fundus photograph (**A**). *Scale bar*: 200 μm. (**C**) Five consecutive frames acquired by AO-SLO correspond to the area outlined in *yellow* in the fundus photograph (A) showing the moving erythrocyte aggregates (*yellow dotted line*). AO-SLO imaging was performed by focusing on the photoreceptor layer to detect the cone mosaic pattern. Numerous bright dots represent cones. Capillaries appear as dark shadows on the bright cone mosaic. The example shown in (**C**) depicts the area of sampling used in this study. *Scale bar*: 100 μm.

ocular aberrations and provides high-resolution retinal images that capture photoreceptors,[20] blood flow,[21,22,28] blood corpuscles,[23,24] capillary networks,[25] retinal wall,[26] and the retinal nerve fiber layer.[27] Considering that early retinal diabetic changes originate from microcirculatory disturbances,[29] AO-SLO, which can be used to observe blood corpuscles in the parafovea directly, could be used to evaluate retinal hemorheology in capillary networks. Herein, we analyzed the characteristics of erythrocyte aggregate movement in parafoveal capillary networks of patients with early-stage DR, directly and noninvasively, using AO-SLO.

METHODS

This study was approved by the Institutional Review Board and the Ethics Committee at Kyoto University Graduate School of Medicine. All aspects of study conduct adhered to the tenets of the Declaration of Helsinki. Written informed consent was obtained from each participant after the nature of the study and the risks and benefits of study participation were thoroughly explained.

Subjects

Adaptive optics scanning laser ophthalmoscopy movies were acquired for 20 healthy Japanese volunteers (mean age ± standard deviation, 36.7 ± 11.5 years; range, 20–61 years); 17 diabetic patients without DR (NDR) (8 type 1 and 9 type 2 patients; 39.9 ± 11.7 years; range, 20–55 years); and 10 diabetic patients with nonproliferative DR (NPDR) (4 type 1 and 6 type 2 patients; 39.9 ± 13.6 years; range, 22–59 years). Diabetes type was determined from internal medical records. The international clinical classification was determined by retinal specialists through indirect ophthalmoscopic fundus examination and slit lamp biomicroscopic fundus. A fundus photograph was obtained for all patients.[30] The exclusion criteria were as follows: contraindication to pupil dilation, best-corrected visual acuity worse than 20/25, refractive error > 5.0 or < –6.0 diopters, axial length > 26 mm, intraocular pressure > 21 mm Hg, macular edema, bilateral difference on the stage of DR, prior ocular surgery, hypertension, secondary DM, and pregnancy. All subjects were dilated before AO-SLO image acquisition with 1 drop of tropicamide (0.5%) and phenylephrine hydrochloride (0.5%). Following pupil dilation, subjects were examined for approximately 20 minutes in total per eye while they remained in a seated posture.

Adaptive Optics Scanning Laser Ophthalmoscopy Imaging

The AO-SLO system developed by Canon (Canon, Inc., Tokyo, Japan)[23,24,31] is composed of the AO system, a high-resolution confocal SLO imaging system, and a wide-field imaging subsystem. The imaging wavelength was 840 ± 25 nm, and the wavelength of beacon light for the measurement of wave front aberrations was 760 ± 5 nm. The imaging light and the beacon light were set at 330 and 40 μW, respectively, by calculating the incident power of both light sources in

accordance with the safety limits set by the American National Standards Institute.[32] Multiple high-resolution retinal videos were acquired from the eyes until the entire parafoveal area had been imaged. Videos were recorded for 2 to 4 seconds per scan area, with a field size of $1.4 \times 2.8°$, and were collected for each subject to cover the parafoveal areas. AO-SLO videos from the temporal and nasal areas located 0.25 to 0.5 mm from the foveal center were chosen for analysis, and all observed erythrocyte aggregates were used for analysis. All erythrocyte aggregate velocities were analyzed on movies recorded at a rate of 64 frames/s. All AO-SLO imaging was performed with the optical focus on the photoreceptor layer.[23,24] All target vessels were free of bifurcations within the imaged area. As reported previously,[33] axial length measurements were obtained using an optical biometer (IOL Master; Carl Zeiss Meditec, Dublin, CA, USA). The AO-SLO image angle was converted to the actual distance to the retina based on each subject's measured axial length using the AO-SLO Retinal Image Analyzer (ARIA; Canon, Inc.) software dedicated to our prototype AO-SLO. Adaptive optics imaging and ocular grading were conducted on the same day, in the morning.

Blood Component Discrimination in Adaptive Optics Scanning Laser Ophthalmoscopy Videos

The transparency of leukocytes to the AO-SLO laser enables leukocytes to be identified as bright, moving objects, which represent light reflected from the photoreceptors within the optical focus of the photoreceptor layer. The AO-SLO laser does not pass through erythrocyte aggregates, which are depicted as black moving objects.[23] Blood components were identified using spatiotemporal (ST) images, according to the methods proposed by our previous report.[28] Briefly, leukocyte traces were identified as follows: thick, high contrast, sparse, and unidirectional. Plasma gap traces, which tended to have lower contrast than leukocyte traces, were identified as thin and dense. Erythrocyte aggregate traces following leukocyte traces were identified as thick, high contrast, and hyporeflective.[24]

Evaluation of the Rheological Properties of Erythrocyte Aggregates

Velocity Measurement. We investigated the aggregated erythrocytes that blocked the AO-SLO laser, creating shadows. Erythrocyte aggregates were described as dark regions (darker than the vessel shadow) that occurred closely behind leukocytes (Supplementary Movie S1). Considering that the erythrocyte aggregates followed the leukocytes, the velocity for the head of the erythrocyte aggregate was equivalent to the velocity of the leukocyte's tail end. The method used to measure velocity has previously been described in full.[24] Briefly, ST images for AO-SLO movies on the target vessels, which were free from bifurcations, showed a white band and black band corresponding primarily to the trajectories of moving leukocytes and erythrocyte aggregates, respectively (Fig. 2). The head end of erythrocyte aggregate velocities, which was equivalent to the tail end of leukocyte velocities on ST images, was obtained by calculating the reciprocal of the slope of the borderline between the white and black bands depicted in the ST image. In order to synchronize velocity and cardiac pulsation, a pulse oximeter (Oxypal Neo; Nihon Kohden, Tokyo, Japan) was attached to the subject's earlobe. Referring to the Martin et al.[22] report, the measurements were divided into five equal bins, each corresponding to the segment of the cardiac cycle in which they were observed to correct for the influence of cardiac pulsation on measured velocities (Fig. 3). The overall average velocity of all five bins was then calculated by averaging the mean velocities of individual bins. The pulsatility index (PI) was calculated as follows, according to the methods proposed by Tam et al.[34]

$$\mathrm{PI} = \frac{V\mathrm{max} - V\mathrm{min}}{V\mathrm{mean}} \quad (1)$$

where PI, V_{max}, V_{min}, and V_{mean} represent pulsatility index, the maximum velocity of individual bins, the minimum velocity of individual bins, and the overall average velocity of individual bins, respectively. The velocities for microaneurysm and tortuosity in NPDR group are not included for analysis to exclude the direct influence of turbulent flow.

Erythrocyte Aggregate Elongation Rate Analysis. The elongation of erythrocyte aggregates in a time-dependent manner in the parafoveal capillaries is a normal finding that can be observed in healthy subjects.[24] In the current study, the elongation rate of erythrocyte aggregates was calculated by means of ST images, as described in our previous paper (Fig. 4).[24]

Reproducibility of the Measurement of Velocity and Erythrocyte Aggregate Elongation Rate. In order to evaluate the reproducibility of the measurement of velocity and erythrocyte aggregate elongation rate, the same vessels in five normal subjects were analyzed on 3 different days within a period of 2 months.

Categorization of Spatiotemporal Images. The characteristics of ST images were compared among the groups to analyze the associated rheological properties. Further observation of ST images for the vessel containing the erythrocyte aggregates made it possible to categorize the ST images into four groups (Fig. 2). The patterns were categorized into the following types: (1) white and black bands that gradually widened, (2) white and black bands that started wider than type 1 bands and then increased in width, (3) both bands exhibited minor changes in width, (4) band slope bent concavely or convexly while traveling through a vessel free of bifurcations, which meant that the velocities changed in a time-dependent fashion. The ST images were categorized by two ophthalmologists after visual inspection. The assessment was performed with the assessors blinded to participant information. When the categorization differed among the assessors, the type was determined based on a discussion with reference to the AO-SLO movies.

Statistical Analyses

All values are presented as mean ± standard deviation. Comparisons of the ages, average velocities of erythrocyte aggregates, maximum velocities of individual bins, minimum velocities of individual bins, elongation rate of erythrocyte aggregates, and pulsatility index among the groups were carried out using 1-way ANOVA, with post hoc comparisons tested using the Scheffe test. The difference in the characteristics between patients without diabetic retinopathy and those with nonproliferative diabetic retinopathy as well as the difference in the HbA1c levels between the NDR and NPDR groups were analyzed using a Mann-Whitney U test. The relationships between the erythrocyte aggregate velocities and HbA1c and between erythrocyte aggregate elongation rate and HbA1c were analyzed using the Pearson correlation coefficient. The velocity and erythrocyte aggregate elongation rate measurements performed on three different days were compared using repeated-measures ANOVA. Comparisons of velocities over the pulse cycle among the normal group, NDR group, and NPDR group were carried out using repeated-measures ANOVA. All analyses were performed using StatView (Version 5.0; SAS Institute, Cary, NC, USA). A P value < 0.05 was considered statistically significant.